J Appl Electrochem (2013) 43:667–677
DOI 10.1007/s10800-013-0563-0

ORIGINAL PAPER

Preparation of Ag–Cu bimetallic dendritic nanostructures and their hydrogen peroxide electroreduction property

Yarong Kang · Fuyi Chen

Received: 3 March 2013 / Accepted: 9 May 2013 / Published online: 16 May 2013

Abstract In this work, dendritic silver–copper (Ag–Cu) nanostructures were synthesised on a copper foil by electrodeposition and subsequently galvanic displacement reaction without any surfactant. The crystalline nature of the nanostructures was examined by X-ray diffraction, and the morphology of the material was investigated by field-emission scanning electron microscopy. The applied potential, displacement reaction time, and silver nitrate solution concentration exerted different effects on the nanoparticle shape. And a possible growth mechanism of the Ag–Cu dendrites was proposed based on the experimental results. The electrochemical properties of the Ag–Cu dendrite-modified electrode were characterised by linear sweep voltammetry. The reduction peak potential of hydrogen peroxide (H_2O_2) was about −0.25 V (vs. a saturated calomel electrode), which indicated that the as-synthesised Ag–Cu dendrites had favourable electroreduction activity towards hydrogen peroxide. At the same time, we found that the solution pH also affected the electrocatalytic ability of the dendrites for H_2O_2 reduction, which was important for the design of a $NaBH_4$–H_2O_2 battery.

Keywords Electrodeposition · Silver–copper nanodendrites · Hydrogen peroxide · Electrocatalysis

Y. Kang · F. Chen (✉)
State Key Laboratory of Solidification Processing, Northwestern Polytechnical University, Xian 710072, People's Republic of China
e-mail: fuyichen@nwpu.edu.cn

1 Introduction

Fuel cells are a promising power-generation technology for the direct conversion of chemical energy into electricity. They play crucial roles in solving the problems of energy crisis and environment pollution. Platinum (Pt)-based catalysts critically determine the efficiency and cost of fuel cells [1]. Given the remarkable physicochemical properties of noble metals in the Pt group, they are considered as the best catalysts for electrochemical reaction [2–5]. However, the cost of these noble metals hinders the commercialisation of noble metal catalysts. According to New York Mercantile Exchange on 16 October 2012, the prices of Au, Ag, Cu, Pt, and Pd were USD 1746, 33, 0.25, 1645, and 639 per troy ounce, respectively [6]. Pt-based catalysts alone account for 38–56 % of the cost of polymer electrolyte membrane fuel cells, and the cathode consumes around 90 % of Pt catalysts because of its sluggish oxygen reduction reaction (ORR) kinetics. Accordingly, recent studies have focused on developing new catalysts to find alternative, low-cost materials and improve the utilisation of fuels cells.

Zhao et al. [7] improved the utilisation of Pt and ultimately decreased the cost by depositing very small Pt particles or clusters onto Au nanoparticles about 10 nm in size, and then loading the Pt@Au particles onto a conventional carbon support. Tian et al. [8] synthesised tetrahexahedral Pt nanocrystals with high-index facets and studied their electro-oxidation activity. They found that these high-energy surfaces are thermally (800 °C) and chemically stable, and exhibited highly enhanced (400 %) catalytic activity for equivalent Pt surface areas in the electro-oxidation of small organic fuels.

Alloys can also be used to decrease the cost of fuel cells. Several assemblies of bimetallic materials have been

synthesised, including Au–Pd [9], Cu–Pd [10], and Ni–Mo [11]. Considering the lower cost and similar electronic structure to Pt, the bimetallic Ag and Cu nanoalloys are potential alternative catalysts for Pt. Xia et al. [12] prepared dendritic Ag nanostructures by electrodeposition and found that these dendrites have a good H_2O_2 electroreduction ability and can used as H_2O_2 sensors. Qiu et al. [13] prepared unique heterogeneous Cu dendrites by a surfactant-free electrochemical method and studied their NO_3^- and H_2O_2 catalysis properties.

Generally, the size, shape, and morphology of metal nanostructures are closely related to material's properties and applications [14–18]. Among various specific nanostructures, dendritic materials with remarkable hierarchical structures and potential applications in the catalysis and technological fields have attracted considerable attention [19–21]. To date, various methods of fabricating dendritic metal nanostructures have been developed, including electrochemical, chemical, and physical methods. The electrochemical method is traditionally used to obtain noble metal dendrites or thorn nanostructures such as Pt, Ag, and Au dendritic nanostructures [22–24]. However, this method is defective when it is used to synthesise alloys because of its different deposition potentials for different metals. Ag–Cu alloy is a good example. Considering the significantly different deposition potentials of Ag and Cu, Ag–Cu bimetallic dendritic nanostructures are difficult to synthesise by electrochemical deposition. However, several studies have indicated that bimetallic nanoparticles (composed of two different metal elements) are of greater interest than monometallic nanoparticles in improving the optical and catalytic properties of metal particles. Bimetallisation can improve the performance of the original pure single-metal nanoparticle and create a new property that may not be achieved by monometallic particles. This synergistic effect is very important in the electrocatalytic performance of metallic particles. Thus, a high-quality method for the large-scale preparation of Ag–Cu bimetallic dendritic nanostructures and the determination of their growth mechanism require further study.

In this work, well-defined Ag–Cu dendritic nanostructures were synthesised by electrodeposition and subsequently galvanic displacement reaction without any surfactant. No further chemical treatment or special technique was needed to affix the catalyst onto the electrode surface. The shape and size of the nanoparticles were readily controlled by adjusting the preparation conditions (working electrode potential, Ag ion concentration, and time). A possible growth mechanism of the Ag–Cu dendrites was proposed based on the experimental results. The electroreduction ability of H_2O_2 was also demonstrated by electrochemical measurements, which indicated that the as-synthesised Ag–Cu dendrites had favourable electroreduction activity towards hydrogen peroxide.

2 Experimental methods

2.1 Preparation of Ag–Cu nanodendrite

Cu was electrodeposited in a three-electrode cell using a CHI660C electrochemical workstation. A Pt electrode was used as the auxiliary electrode (anode), and a saturated calomel electrode (SCE) was used as the reference electrode. All potentials reported in this work were versus the SCE reference electrode unless otherwise specified. The electrolyte solution was composed of 10 mM $CuSO_4$ (Tianjin Yaohua Chemical Reagent Co.) and 10 mM $NaClO_4$ (Tianjin Fuchen Chemical Reagent Factory). A highly purified Cu foil (5 cm × 1 cm) was used as the substrate for electrodeposition. The foil was first burnished by 1,000 and 2,000 cw abrasive paper and then cleaned with ethanol, diluted sulphuric acid, and deionised water in an ultrasonicator for 10 min. Amperometric current–time (*I–t*) curves were constructed to obtain the depositions from the mixture solution at different working potentials (e.g. −0.2, −0.5, −0.6, or −0.8 V). The area used for deposition was 1 cm^2, and the remaining area was coated with nail polish. After a certain time of electrolysis, the electrode was removed and washed with deionised water several times.

After washing with deionised water and air drying, the fresh Cu particles were immediately immersed in $AgNO_3$ solution (e.g. 1, 5, 10, or 20 mM) for different times in the dark to avoid Ag photoreduction. The resulting Ag–Cu dendrites were then rinsed with water carefully to prevent them from breaking.

2.2 Characterisation of dendritic structure

To determine the crystalline nature of the Ag–Cu nanostructures, X-ray diffraction (XRD) patterns were recorded using a X-Per-PRO diffractometer with Cu K_α radiation ($\lambda = 1.5418$ Å). The work potential and current were 40 kV and 40 mA, respectively. The morphologies of the samples were studied by a field-emission scanning electron microscopy (SEM) system (JSM-6390). Electrochemical measurements were taken using a CHI660C electrochemical workstation at room temperature. Cyclic voltammetry (CV) experiments were performed to obtain the right deposition potential of Cu foam. Electrolyte solutions were used as described above. To estimate the H_2O_2 electroreduction ability, the electrodes modified by the Ag–Cu dendritic material were tested by linear sweep voltammetry

(LSV). The CV and LSV scanning rates were set to 50 mV/s.

3 Results and discussion

3.1 Electrodeposition and morphology of Cu on a Cu foil

Voltammetric technique is a very useful tool to establish the main features of a deposition process. In this paper, CV was used to monitor the redox behaviour of Cu^{2+} at a Cu electrode. As shown in Fig. 1a, the scanning rate was 50 mV/s, the initial potential was 0 V, and the scanning direction was from 0 to −1 V and to 1 V. In the solution containing 10 mM $CuSO_4$ and 10 mM $NaClO_4$, the electrode showed a cathodic peak at −0.53 V and no anodic peak was observed in the circulation. The cathodic peak was related to the reduction of Cu^{2+}. To determine the reasons for the absence of the oxidation peak, the same test was conducted on an indium tin oxide (ITO) glass (Fig. 1b) and a sharp anodic peak of about 0.76 V was found. Therefore, it was indicated that the electrode reaction was irreversible on the copper foil. The copper crystals, which produced during negative scan (that is the scanning direction to negative potential), were oxidised after a period of the positive scan (that is the scanning direction to positive potential) beginning. After the electrodeposited Cu was oxidised, the clean surfaces of Cu foil continued to be oxidised and exhibited linear increase in the oxidation current. This phenomenon caused the dissolution of deposited crystal Cu and Cu foil but without a visible oxidation peak. By contrast, electric sediments on ITO glass started to be oxidised when electrode potential crosses the equilibrium potential. Response current increased continuously until reached the peak of the oxidation current (at 0.76 V), then current decreased due to the reducing of surface-active substances. So reduction occurs below equilibrium potential on the substrate of ITO glass and Cu foil, at the same time oxidation above equilibrium potential. From the Fig. 1, the equilibrium potential of ITO glass and Cu foil was about −0.1 and −0.2 V, respectively. According to the above analysis, the Cu ions on the Cu foil electrode considerably decreased within the range of −0.1 to −1 V due to electroreduction. As we know, electrode potential determines the electrodeposition process of nucleation and growth kinetics, and overpotential is the driving force of nucleation. So the deposition potential was reasonably established, the Cu-modified electrode could be obtained by the following electrodeposition potentials at −0.2, −0.5, −0.6, or −0.8 V in order to check the effect of the potential on the morphology.

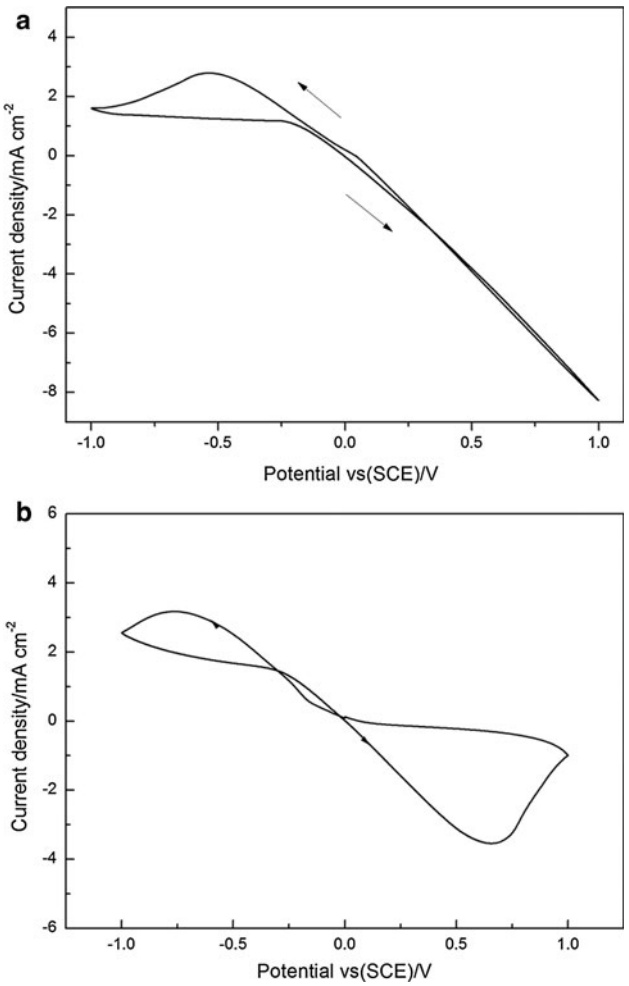

Fig. 1 Cyclic voltammograms on **a** the Cu foil electrode and **b** ITO glass in a solution containing 10 mM $CuSO_4$ + 10 mM $NaClO_4$ at a scan rate of 50 mV/s

Figure 2 shows the *I–t* curves at different electrolysis potentials. The change in reduction current was consistent with the CV results. The reduction current increased with increased negative potential shift and then decreased beyond the peak potential (−0.6 V). During the electrolysis process, the applied potentials were very crucial to the occurrence of the reaction $Cu^{2+} + 2e^- = Cu$ (E^θ = 0.337 V vs. SHE) on the working electrode. The main reason was that overpotential is the electrochemical driving force in the constant potential mode [25], significantly affecting the nucleation and growth kinetics and, ultimately, the morphology. Metal deposition is a process of nucleation and crystal growth. Overpotential affects the nucleation probability directly and has the following formula:

$$w = B\exp\left(-b/\eta_k^2\right) \quad (1)$$

where the w is nucleation probability, η_k is overpotential, and B, b are constant. To illustrate this point, the samples

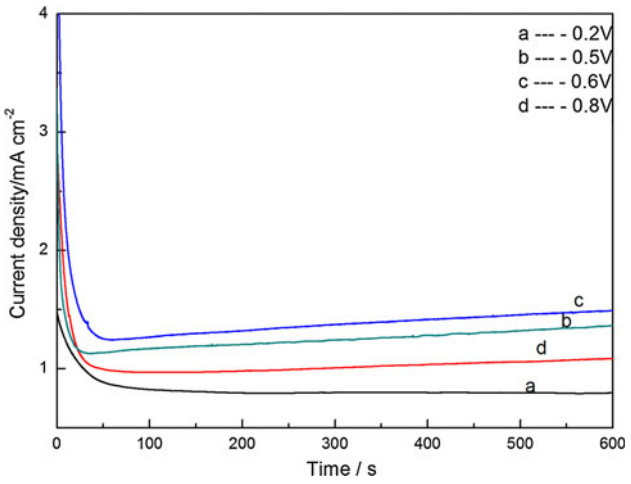

Fig. 2 *I–t* curves of different potentials of **a** −0.2, **b** −0.5, **c** −0.6, or **d** −0.8 V (vs. SCE) with Cu ion at a concentration of 10 mM for an electrolysis time of 600 s

obtained at different potentials at a constant Cu ion concentration (10 mM) were analysed by SEM and the results are shown in Fig. 3. The morphology differed among different potentials, but a distinct trend can be observed. Materials obtained at a low potential (Fig. 3a, −0.2 V) only had a few small rod-shaped particles and no dendritic structure. This finding can be attributed to two reasons. On the one hand, the stable nuclei are too small to grow. On the other hand, the almost equal rates of oxidation and reduction at low overpotential, making less Cu ions reduced and spread to the nucleation surface and growth. At more negative potentials of −0.5 and −0.6 V, a branched crystal structure was observed and the dendritic structures were larger, more abundant, and had a well-defined morphology (Fig. 3b, c). Therefore, electron transfer was faster at a high applied potential and more Cu^{2+} was rapidly reduced to form Cu dendrite by mass transfer. At higher potentials, the growth rate was expected to be faster. Interestingly, when the potential was further increased to −0.8 V, the dendritic Cu crystals disappeared and were replaced by Cu foam (Fig. 3d). When the applied potential was higher than the peak potential, the current density rapidly decreased, as shown in the CV and *I–t* curves. Thus, fewer metal ions were reduced on the substrate per unit of time. At the same time, according to the formula (1), more stable nucleus was formed and evenly grew into foam due to a sluggish response of mass transfer.

3.2 Characteristics of Ag–Cu dendritic nanostructures

After deposition, the Cu foil was immersed in $AgNO_3$ aqueous in the dark to avoid Ag photoreduction. Several minutes later, Ag–Cu bimetallic nanostructures were synthesised by a galvanic displacement and primary battery reaction. Figure 4 shows the XRD pattern of the as-

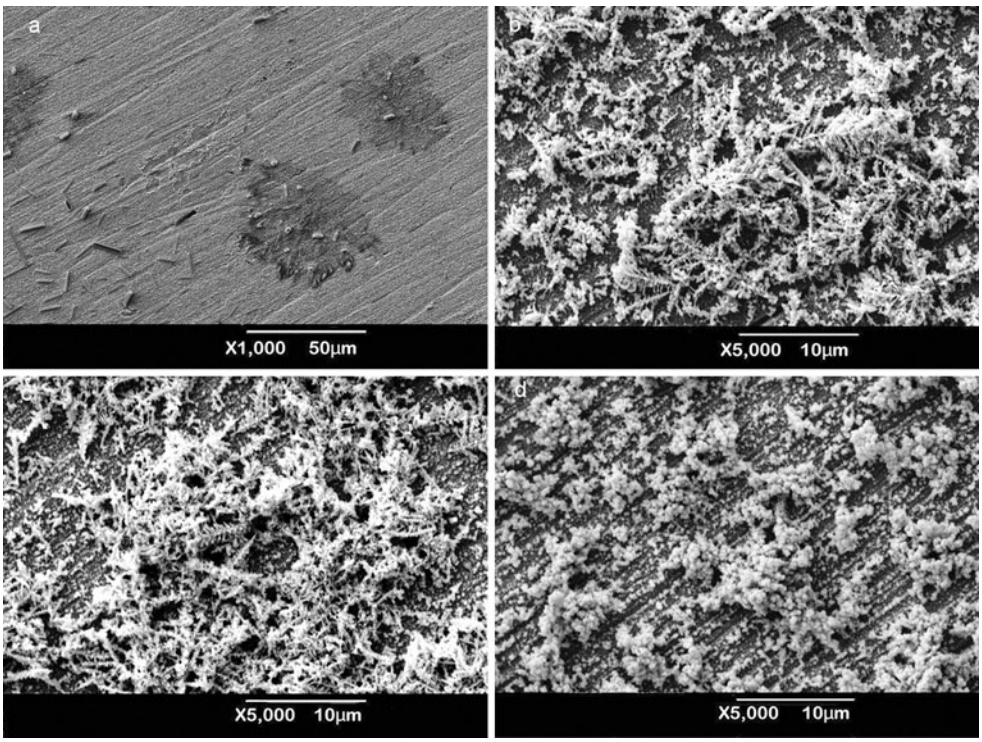

Fig. 3 Typical SEM images of Cu nanostructures obtained at different potentials: **a** −0.2, **b** −0.5, **c** −0.6, and **d** −0.8 V versus SCE. The electrolysis was carried out for 600 s at a Cu ion concentration of 10 mM

synthesised sample. All diffraction peaks are marked in the image. The (111), (200), (220), (311), and (222) diffraction peaks of the cubic structure of metallic Ag indicated the crystalline nature of Ag in the dendrite [26]. The (111), (200), (220), and (311) diffraction peaks of the cubic structure of metallic Cu indicated the crystalline nature of Cu in the dendrite [13]. The presence of Cu_2O peaks can be attributed to the oxidation of Cu foam before galvanic displacement reaction. The XRD spectrum confirmed the crystallinity of the dendritic structures but the specific composition and structure were still unknown for effecting of substrate. More works need to be done. Fortunately, Chen et al. [27] have done some research and concluded that the composition of the dendrites grown from the Cu substrate by galvanic displacement was not pure Ag but Ag–Cu from the measurement of selected-area electron diffraction, energy-dispersive X-ray line scans, and X-ray photoelectron spectroscopy. To reduce the influence of the substrate, the experiment only scanned the sample surface.

To determine the morphological relationship between the Cu precursor and Ag–Cu dendritic nanostructure, the Cu precursor samples obtained at different electrolysis potentials (−0.6, −0.7, and −0.8 V) with the other conditions fixed were subjected to SEM analysis, and the results are shown in Fig. 5. Although the Cu precursor morphology changed from dendritic to foam-like at the different deposition potential, as shown in Fig. 3, the synthesised Ag–Cu materials show the uniform and fine dendritic structures and the dendrite coverage on the electrode surface increased with increased potential. The leaves of the primary dendrites were large and no other branch was found (Fig. 5a, b). At a more negative potential of −0.7 V, secondary dendrites began to grow (Fig. 4c, d). When the potential reached an even more negative value, secondary dendrites grew well and the arm spacing became narrow.

The concentration significantly affects the morphology of Ag dendrites [28]. The typical SEM images of Ag–Cu nanostructures obtained at different Ag ion concentrations and a fixed reaction time (10 min) are shown in Fig. 6. Cu foam was obtained by electrolysis for 600 s at a potential of −0.8 V versus SCE. Lamellar structures were observed at a low concentration of 1 mM, whereas some crystals tended to branch (Fig. 6a, b). The material obtained at an Ag ion concentration of 5 mM aggregated and began to grow sparse and imperfect dendrites (Fig. 6c, d). At a higher concentration of 10 mM, the dendrites uniformly formed and covered the entire electrode surface; subsequently, secondary branches emerged (Fig. 6e, f). When the concentration was increased to 20 mM, more dense dendrites with larger dimensions were observed and only a few secondary dendrites were formed (Figs. 6g, h). These results indicated the important role of the Ag ion concentration in the formation and growth of Ag–Cu nanoparticles.

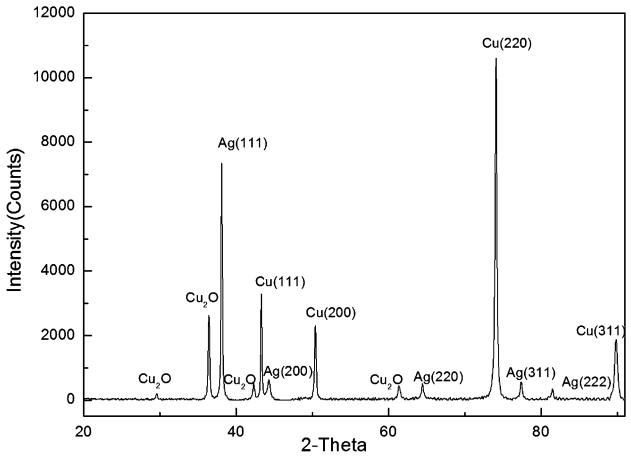

Fig. 4 XRD pattern of Ag–Cu dendrites. The sample was obtained at an applied potential of −0.8 V with an electrolysis time of 600 s and displacement reaction time of 10 min in an aqueous solution containing 10 mM $AgNO_3$

The electrolysis potential of Cu, as well as the Ag concentration significantly affected the morphology of Ag–Cu nanoparticles. To determine whether the reaction time of galvanic displacement also affected the growth of dendrites, a series of experiments was conducted. In these experiments, all conditions were fixed except for the reaction time of galvanic displacement. The typical SEM images of the nanostructures obtained are shown in Fig. 7. The reaction time had little influence on the morphology. All materials developed into dendrites whose dimensions only slightly differed with prolonged reaction time.

The above analyses revealed that the applied potential of electrolysis and Ag concentration considerably affected the morphology of Ag–Cu dendrites compared with the electrolysis time and galvanic reaction time. Thus, a tentative two-stage mechanism is hereby proposed. First, Cu foam was synthesised through electrochemical reaction and crystallisation. Second, Ag–Cu dendrites were formed by the reaction of galvanic displacement and primary batteries. In the process of Cu formation, Cu ion was rapidly reduced to form Cu atoms through an electron transfer reaction by a driving force (the applied potential). Large quantities of Cu then aggregated by the surface diffusion of atoms. When Cu foam made contact with the $AgNO_3$ solution, the galvanic displacement reaction immediately occurred to form Ag atoms and Cu ions. The Ag nanoparticles and Cu foam subsequently generated numerous nanometre-scale cells based on the primary battery mechanism. In this process, a mass of Cu nanoparticles formed a negative electrode and decayed into Cu^{2+}, releasing electrons that subsequently travelled to the positive electrode. In the Cu^{2+}/Ag^{+}-containing electrolyte, Cu^{2+} and Ag^{+}

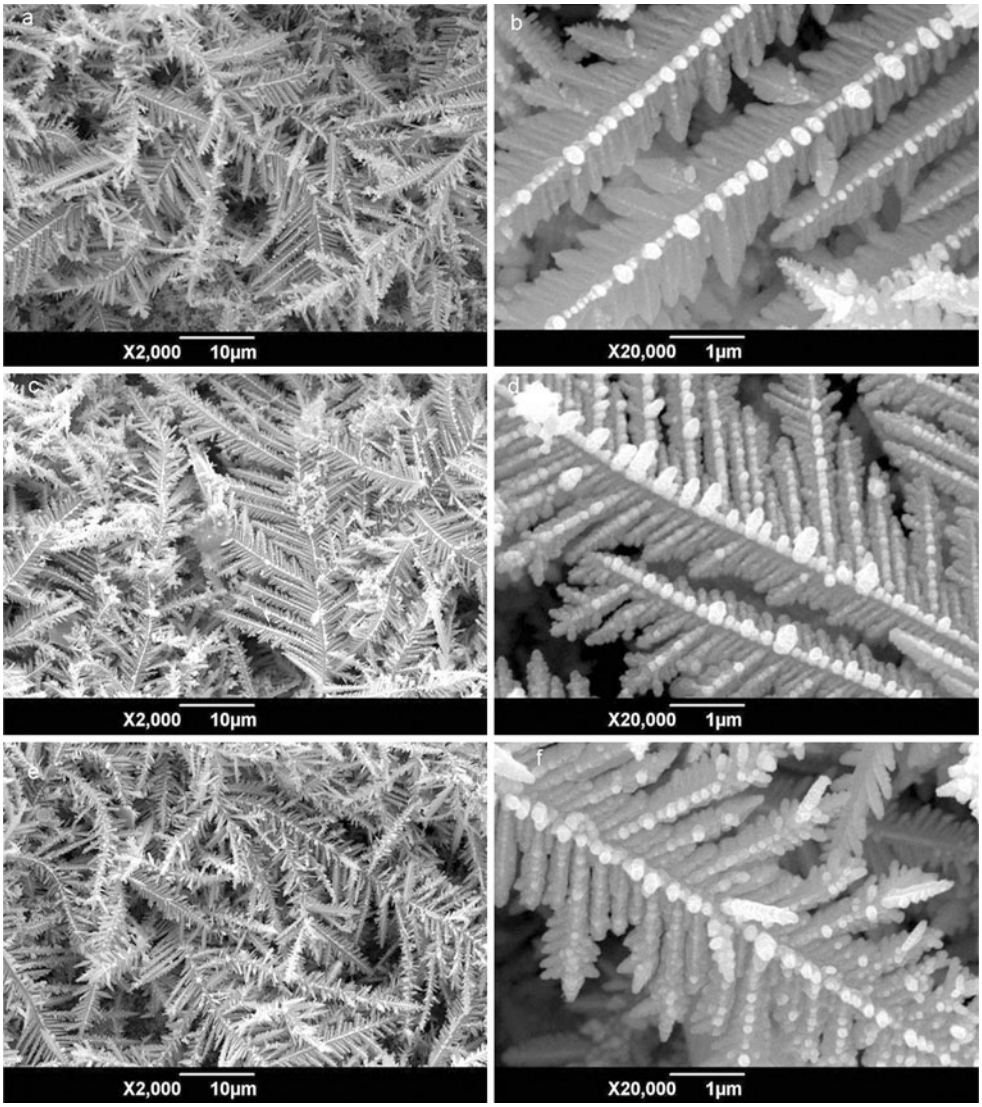

Fig. 5 Typical SEM images of Ag–Cu nanostructures obtained at different Cu ion deposition potentials: **a**, **b** −0.6, **c**, **d** −0.7, and **e**, **f** −0.8 V versus SCE. The electrolysis time is 600 s, Ag ion concentration is 10 mM, and the displacement reaction time is 10 min

ions moved into the cathode. Apart from the reduction reaction of Ag^+, Cu^{2+} was reduced and the Cu phase regenerated along with Ag formation. The increase in Cu^{2+} ion concentration caused by the galvanic displacement further promoted the reaction, which led to the deposition of the regenerated Cu nanoparticles onto the surface of Ag dendrites. Subsequently, the growth of Ag and Cu structures occurred, and the dendrites formed with the continuous replacement [27].

3.3 H_2O_2 electroreduction and performance of the H_2O_2 sensor

H_2O_2 is an extremely important compound because of its wide-ranging applications in many research fields. It also has excellent storability, which is considerably beneficial to the development of $NaBH_4$–H_2O_2 fuel cells, and the reducing property of H_2O_2 when used as cathode fuel in an $NaBH_4$–H_2O_2 fuel cell significantly depends on the solution pH. When the cathode is alkaline, the reaction is as follows, with the theoretical cell potential of 2.11 V and specific energy of 11,959 Wh/kg:

$$4\ H_2O_2 + 8e^- \rightarrow 8\ OH^-, E^\theta = 0.87\ \text{V vs. SCH} \quad (2)$$

$$\text{Cell reaction}: BH_4^- + 4\ H_2O_2 \rightarrow BO_2^- + 6\ H_2O \quad (3)$$

When H_2O_2 reduction occurs in an acidic medium, the cathode reaction is as follows: the theoretical cell potential and specific energy are 3.01 V and 17,060 Wh/kg, respectively. [29]

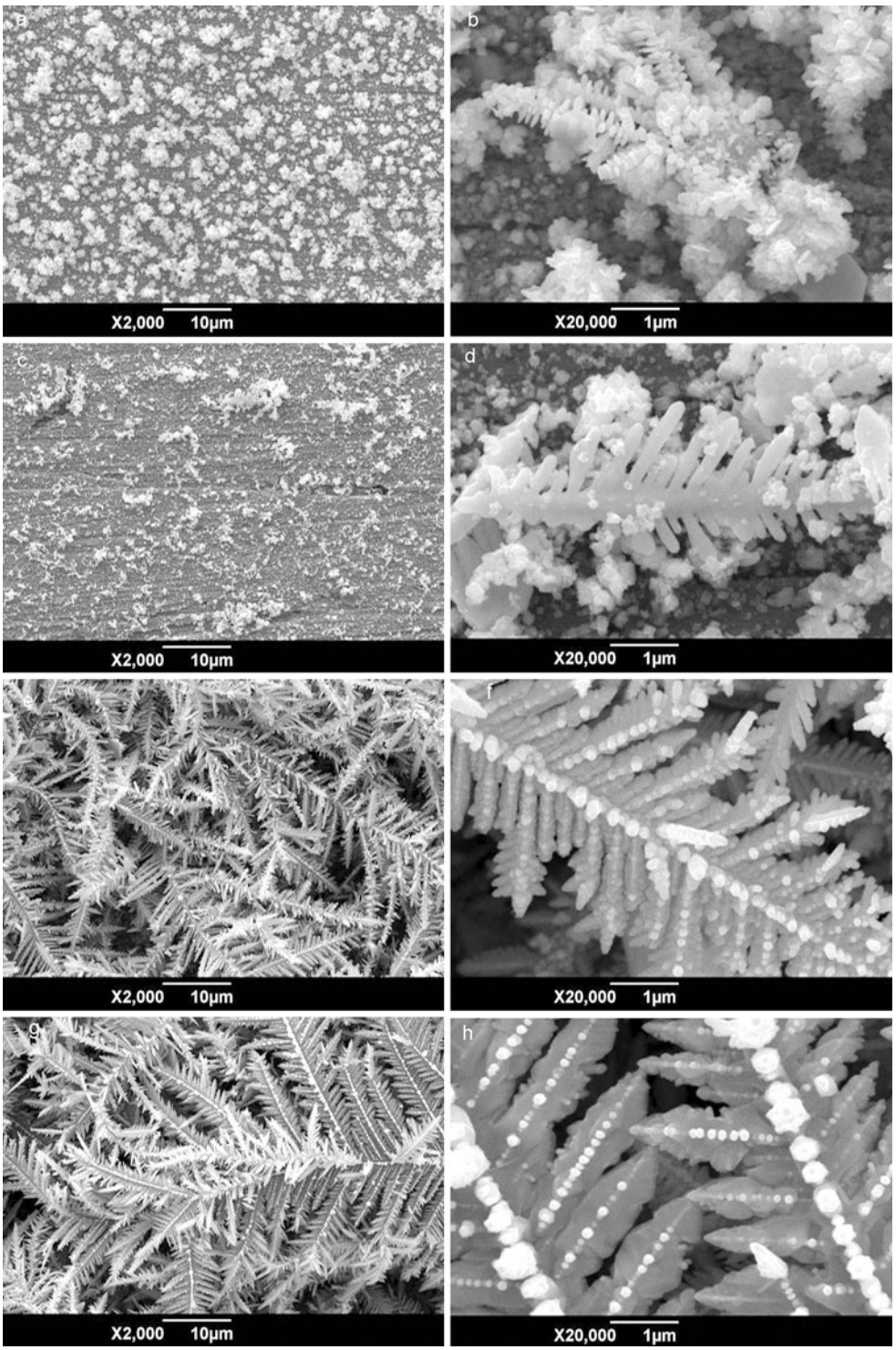

Fig. 6 Typical SEM images of Ag–Cu nanostructures obtained at different Ag ion concentrations with at a fixed reaction time (10 min): **a**, **b** 1, **c**, **d** 5, **e**, **f** 10, and **g**, **h** 20 mM. The electrolysis of Cu was carried out for 600 s at a potential of −0.8 V versus SCE

$$4\ H_2O_2 + 8\ H^+ + 8\ e^- \rightarrow 8\ H_2O, E^\theta = 1.77\ \text{V vs. SCH} \quad (4)$$

$$\text{Cell reaction}: \ BH_4^- + 4\ H_2O_2 \rightarrow BO_2^- + 6\ H_2O \quad (5)$$

H_2O_2 has great potential use as cathode fuel in $NaBH_4$–H_2O_2 fuel cells. Compared with the anode hydrogen oxidation reaction, the cathode ORR is six or more orders of magnitude slower, which limits its performance. Thus, several studies have focused on improving cathode catalysts. To date, most studies on cathode catalysts for H_2O_2 focus on noble metals, alloys, and metal oxides. To

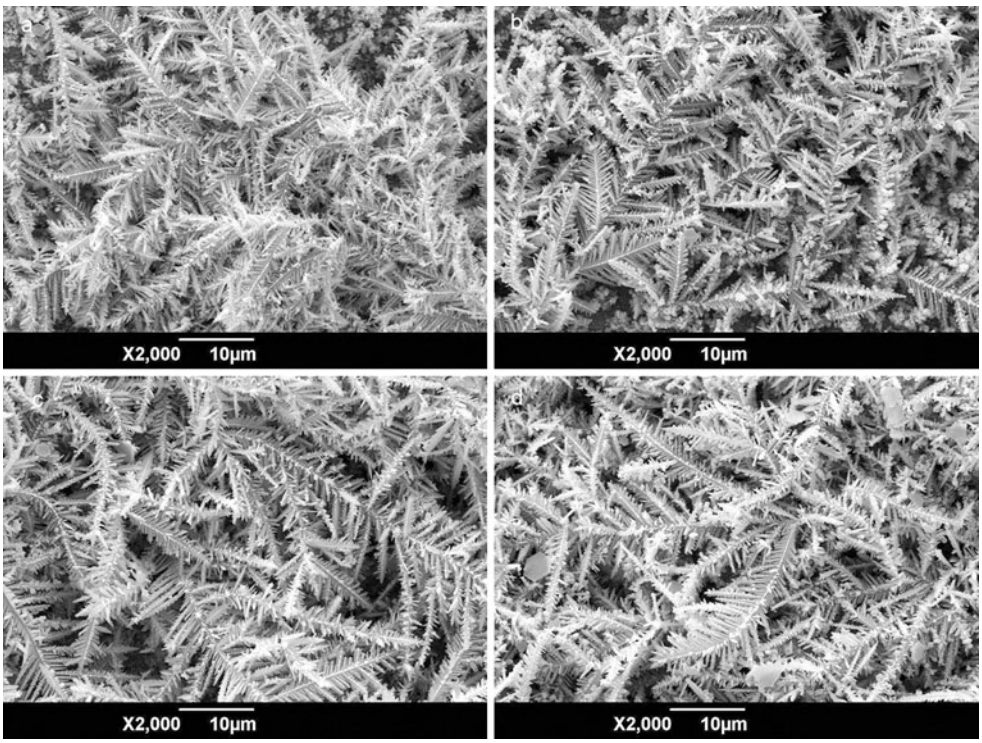

Fig. 7 Typical SEM images of Ag–Cu nanostructures obtained at different galvanic displacement reaction times at a fixed Ag concentration (10 mM): **a** 5, **b** 10, **c** 20, and **d** 30 min. The electrolysis of Cu was carried out for 600 s at a potential of −0.8 V versus SCE

evaluate the applicability of the Ag–Cu dendrites as an electrode material, the electroreduction ability of the Ag–Cu dendrite-modified electrode towards H_2O_2 in phosphate-buffered saline (PBS) was examined. PBS with different pH values was prepared from disodium hydrogen phosphate and sodium dihydrogen phosphate (Tianjin Fuchen Chemical Regents). Figure 8 shows the LSV curves of Cu dendrite electrode and Ag–Cu dendrite-modified electrode in an aqueous solution containing 0.025 M PBS (saturated with N_2, pH 6.86) and 5 mM H_2O_2. Both curves (a) and (b) exhibited a large peak near −0.25 V (vs. SCE). This peak can be ascribed to the reduction of H_2O_2, which was much lower than a previously reported Ag NP-modified glassy carbon electrode (GCE; −0.68 V vs. SCE) [30], Ag-DNA/GCE (−0.44 V vs. SCE) [31], and Cu(II)–TPT/GE (−0.29 V vs. SCE) [32]. That indicates a faster electron transfer rate and higher electrocatalytic activity towards the reduction of H_2O_2 at Ag–Cu dendrites. The current density of Ag–Cu dendrite is much higher than that of Cu dendrite at the same potential (peak potential). Due to the same morphology, surface effect can be ignored. So Ag–Cu dendrites have higher catalytic activity than Cu dendrites. However, compared with the pure silver dendrite whose reduction potential towards H_2O_2 is about −0.4 V(vs. Ag/AgCl) [12], Ag–Cu dendrites have a much lower reduction overpotential to H_2O_2, which means Ag–Cu dendrites have higher electrocatalytic activity. Thus, we can conclude that Ag–Cu dendrites have a better catalytic activity than pure Ag dendrites and Cu dendrites attributed to the synergistic effect. In addition, Ag–Cu dendrites have a better activity towards H_2O_2 than metal compound catalyst such as Fe, Co, and Ni. [33–35]. At the same time, compared with other material in place of the noble metal platinum, such as Au and Pd [36, 37], Ag–Cu dendrite material has a clear price advantage. Considering these factors comprehensively, we can draw a conclusion that Ag–Cu dendrites is the most potential to become a new generation catalyst for the reduction of hydrogen peroxide instead of metal platinum.

In addition to the kind of material, the solution pH and dendrite morphology were also found to have a significant effect on the catalytic property for H_2O_2 reduction. Figure 9 shows the LSV curves of H_2O_2 at different pH values of PBS. Notably, the reduction potential negatively shifted with increased pH. Therefore, the solution required a larger overpotential to reduce H_2O_2 under the high pH conditions. Low pH values favour the adsorption of OOH^- [38, 39]. So $NaBH_4$–H_2O_2 fuel cells have a higher standard output voltage when H_2O_2 reduction occurs in an acidic medium.

The H_2O_2 electrocatalytic abilities of Ag–Cu dendrite-modified electrodes obtained at different conditions were different. Generally, smaller dendrite sizes and larger coverage areas lead to better catalytic performance.

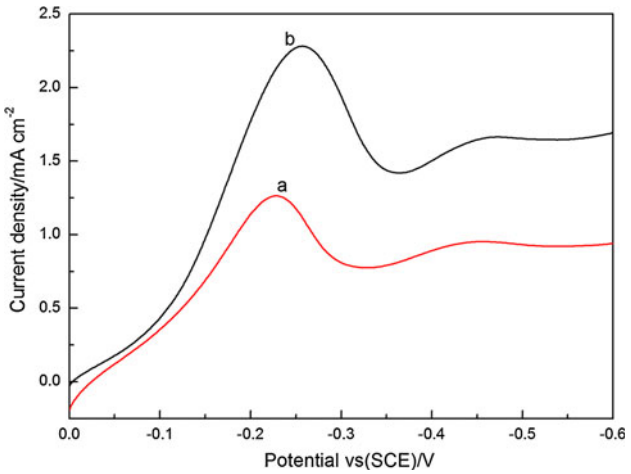

Fig. 8 LSV curves of **a** Cu dendrite electrodes and **b** Ag–Cu dendrite-modified electrodes in a solution containing 0.025 M PBS (pH 6.86) saturated with N_2 and H_2O_2 (5 mM) at a scan rate of 50 mV/s

Figure 10a shows the LSV curves of the modified electrodes obtained at different deposition potentials of Cu (−0.6, −0.7, and −0.8 V). The electrodes modified at more negative potentials exhibited a smaller polarisation potential and a larger peak current. Figure 10b shows the LSV curves for dendrites obtained at different Ag ion concentrations (1, 5, 10, and 20 mM). The electrodes modified with Ag–Cu materials obtained at higher Ag ion concentrations exhibited a larger peak current and negatively shifted polarisation potential. As battery materials, an excessive polarisation potential will decreases its output potential. As shown in Fig. 10b, curve (d) had a much larger negative shift than the others, which suggest we cannot increase Ag concentration without any limit. According to the experimental results, the Ag–Cu dendrite-modified electrodes showed better catalysis when the Ag

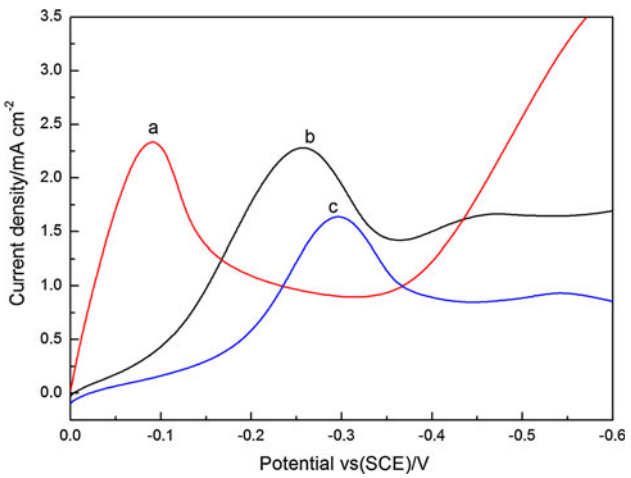

Fig. 9 LSV curves of Ag–Cu dendrite-modified electrodes in PBS saturated with N_2 at **a** pH 2, **b** pH 6.86, and **c** pH 7.8 and H_2O_2 (5 mM) at a scan rate of 50 mV/s

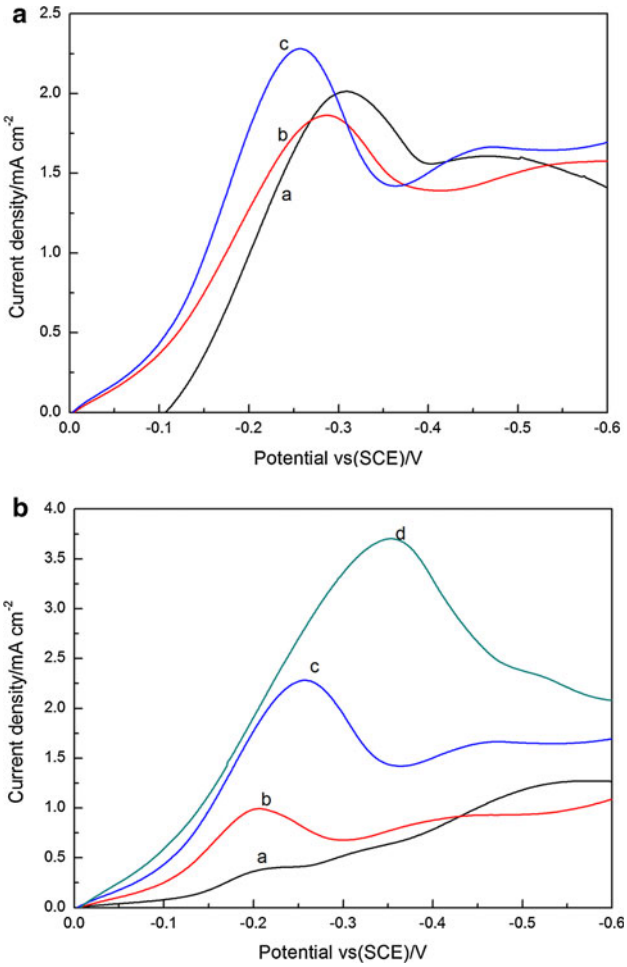

Fig. 10 LSV curves recorded for Ag–Cu dendrite-modified electrodes obtained at **a** different deposition potentials of Cu (*a* −0.6, *b* −0.7, and *c* −0.8 V) and (**b**) different Ag concentrations (*a* 1, *b* 5, *c* 10, and *d* 20 mM) in a solution containing 0.025 M PBS saturated with N_2 (pH 6.86) and H_2O_2 (5 mM) at a scan rate of 50 mV/s

concentration was 10 mM. These results can be attributed to the differences among the effective surface areas of the working electrodes. When the conditions were controlled within a more negative potential and appropriate Ag concentration, Ag–Cu dendrites with a larger effective surface area can be obtained. Larger surface areas allow for more effective electroreduction, as manifested by the reduction potential and current peaks.

4 Conclusion

In summary, heterogeneous Ag–Cu dendrites were synthesised by Cu electrodeposition and the galvanic displacement reaction of $AgNO_3$ aqueous solution with Cu foam at room temperature. The reaction and growth processes were attributed to the galvanic displacement between Cu and Ag^+ ions, as well as the reduction of Cu^{2+}

and Ag^+ ions within primary batteries. The morphology of the Ag–Cu dendrites sensitively depended on the deposition parameters and Ag concentration. The obtained dendritic nanostructures with high surface areas exhibited high electrocatalytic ability for H_2O_2 reduction. The solution pH also affected the electrocatalytic ability of the dendrites for H_2O_2 reduction, which was important for the design of a $NaBH_4$–H_2O_2 battery.

Acknowledgments This study was supported by the National Natural Science Foundation of China (Grant Nos. 51271148 and 50971100), the Research Fund of State Key Laboratory of Solidification Processing in China (Grant No. 30-TP-2009), and the Aeronautic Science Foundation Program of China (Grant No. 2012ZF53073).

References

1. Debe MK (2012) Electrocatalyst approaches and challenges for automotive fuel cells. Nature 486(7401):43–51. doi:10.1038/nature11115
2. Norskov JK, Bligaard T, Rossmeisl J, Christensen CH (2009) Towards the computational design of solid catalysts. Nat Chem 1(1):37–46. doi:10.1038/nchem.121
3. Zhang J, Sasaki K, Sutter E, Adzic RR (2007) Stabilization of platinum oxygen-reduction electrocatalysts using gold clusters. Science 315(5809):220–222. doi:10.1126/science.1134569
4. Anjos DM, Hahn F, Léger JM, Kokoh KB, Tremiliosi-Filho G (2007) In situ FTIRS studies of the electrocatalytic oxidation of ethanol on Pt alloy electrodes. J Solid State Electrochem 11(11):1567–1573. doi:10.1007/s10008-007-0360-y
5. Shao-Horn Y, Sheng WC, Chen S, Ferreira PJ, Holby EF, Morgan D (2007) Instability of supported platinum nanoparticles in low-temperature fuel cells. Top Catal 46(3–4):285–305. doi:10.1007/s11244-007-9000-0
6. Current primary and noble metal price, http://www.metalprices.com/ (Accessed 16 October 2012)
7. Zhao D, Xu BQ (2006) Enhancement of Pt utilization in electrocatalysts by using gold nanoparticles. Angew Chem Int Ed Engl 45(30):4955–4959. doi:10.1002/anie.200600155
8. Tian N, Zhou ZY, Sun SG, Ding Y, Wang ZL (2007) Synthesis of tetrahexahedral platinum nanocrystals with high-index facets and high electro-oxidation activity. Science 316(5825):732–735. doi:10.1126/science.1140484
9. Jirkovský JS, Panas I, Romani S, Ahlberg E, Schiffrin DJ (2012) Potential-dependent structural memory effects in Au–Pd nanoalloys. J Phys Chem Lett 3:315–321. doi:10.1021/jz201660t
10. Hickman AJ, Sanford MS (2012) High-valent organometallic copper and palladium in catalysis. Nature 484(7393):177–185. doi:10.1038/nature11008
11. Chen WF, Sasaki K, Ma C, Frenkel AI, Marinkovic N, Muckerman JT, Zhu Y, Adzic RR (2012) Hydrogen-evolution catalysts based on non-noble metal nickel-molybdenum nitride nanosheets. Angew Chem Int Ed Engl 51(25):6131–6135. doi:10.1002/anie.201200699
12. Qin X, Wang H, Wang X, Miao Z, Fang Y, Chen Q, Shao X (2011) Synthesis of dendritic silver nanostructures and their application in hydrogen peroxide electroreduction. Electrochim Acta 56(9):3170–3174. doi:10.1016/j.electacta.2011.01.058
13. Qiu R, Cha HG et al (2009) Preparation of dendritic copper nanostructures and their characterization for electroreduction. J Phys Chem C 113(36):15891–15896. doi:10.1021/jp904222b
14. El-Sayed MA (2001) Some interesting properties of metals confined in time and nanometer space of different shapes. Acc Chem Res 34(4):257–264. doi:10.1021/ar960016n
15. Qian HS, Antonietti M, Yu SH (2007) Hybrid "Golden Fleece": synthesis and catalytic performance of uniform carbon nanofibers and silica nanotubes embedded with a high population of noble-metal nanoparticles. Adv Funct Mater 17(4):637–643. doi:10.1002/adfm.200600657
16. Rosi NL, Mirkin CA (2005) Nanostructures in biodiagnostics. Chem Rev 105(4):1547–1562. doi:10.1021/cr030067f
17. Xiong YJ, Washio I, Chen JY, Cai HG, Li ZY, Xia YN (2006) Poly(vinyl pyrrolidone): a dual functional reductant and stabilizer for the facile synthesis of noble metal nanoplates in aqueous solutions. Langmuir 22(20):8563–8570. doi:10.1021/la061323x
18. Wang X, Zhuang J, Peng Q, Li YD (2005) A general strategy for nanocrystal synthesis. Nature 437:121–124. doi:10.1038/nature03968
19. Zhou Y, Yu SH, Wang CY, Li XG, Zhu YR, Chen ZY (1999) A novel ultraviolet irradiation photoreduction technique for the preparation of single-crystal Ag nanorods and Ag dendrites. Adv Mater 11(10):850–852. doi:10.1002/(SICI)1521-4095(199907)11:10<850:AID-ADMA850>3.0.:CO;2-Z
20. Zhu LP, Xiao HM, Zhang WD, Yang Y, Fu SY (2008) Synthesis and characterization of novel three-dimensional metallic Co dendritic superstructures by a simple hydrothermal reduction route. Cryst Growth Des 8(4):1113–1118. doi:10.1021/cg701036k
21. Gu CD, Zhang TY (2008) Electrochemical synthesis of silver polyhedrons and dendritic films with superhydrophobic surfaces. Langmuir 24(20):12010–12016. doi:10.1021/la802354n
22. Tian N, Zhou ZY, Sun SG, Cui L, Ren B, Tian ZQ (2006) Electrochemical preparation of platinum nanothorn assemblies with high surface enhanced Raman scattering activity. Chem Commun 39:4090–4092. doi:10.1039/B609164D
23. Geddes CD, Parfenov A, Gryczynski I, Lakowicz JR (2003) Luminescent blinking from silver nanostructures. J Phys Chem B 107(37):9989–9993. doi:10.1021/jp030290g
24. Huang D, Bai X, Zheng L (2011) Ultrafast preparation of three-dimensional dendritic gold nanostructures in aqueous solution and their applications in catalysis and SERS. J Phys Chem C 115(30):14641–14647. doi:10.1021/jp2037284
25. Rezaei B, Damiri S (2010) Electrodeposited silver nanodendrites electrode with strongly enhanced electrocatalytic activity. Talanta 83(1):197–204. doi:10.1016/j.talanta.2010.09.006
26. Wei G, Nan C, Deng Y, Lin Y (2003) Self-organized synthesis of silver chainlike and dendritic nanostructures via a solvothermal method. Chem Mater 15(23):4436–4441. doi:10.1021/cm034628v
27. Chen X, Cui CH, Guo Z, Liu JH, Huang XJ, Yu SH (2011) Unique heterogeneous silver-copper dendrites with a trace amount of uniformly distributed elemental Cu and their enhanced SERS properties. Small 7(7):858–863. doi:10.1002/smll.201002331
28. Qin X, Miao Z, Fang Y, Zhang D, Ma J, Zhang L, Chen Q, Shao X (2012) Preparation of dendritic nanostructures of silver and their characterization for electroreduction. Langmuir 28(11):5218–5226. doi:10.1021/la300311v
29. Demirci UB (2007) Direct borohydride fuel cell: main issues met by the membrane–electrodes-assembly and potential solutions. J Power Sources 172(2):676–687. doi:10.1016/j.jpowsour.2007.05.009
30. Welch CM, Banks CE, Simm AO, Compton RG (2005) Silver nanoparticle assemblies supported on glassy-carbon electrodes for the electro-analytical detection of hydrogen peroxide. Anal Bioanal Chem 382(1):12–21. doi:10.1007/s00216-005-3205-5
31. Wu S, Zhao H, Ju H, Shi C, Zhao J (2006) Electrodeposition of silver–DNA hybrid nanoparticles for electrochemical sensing of hydrogen peroxide and glucose. Electrochem Commun 8(8):1197–1203. doi:10.1016/j.elecom.2006.05.013

32. Dias VLN, Fernandes EN, da Silva LMS, Marques EP, Zhang J, Marques ALB (2005) Electrochemical reduction of oxygen and hydrogen peroxide catalyzed by a surface copper(II)–2,4,6-tris(2-piridil)-1,3,5-triazine complex adsorbed on a graphite electrode. J Power Sources 142(1–2):10–17. doi:10.1016/j.jpowsour.2004.09.032
33. Garjonyè R, Malinauskas A (1998) Electrocatalytic reactions of hydrogen peroxide at carbon paste electrodes modified by some metal hexacyanoferrates. Sens Actuat B 46(3):236–241. doi:10.1016/S0925-4005(98)00123-3
34. Jaouen F, Dodele JP (2009) O2 reduction mechanism on non-noble metal catalysts for PEM fuel cells. J Phys Chem C 113(34):15433–15443. doi:10.1021/jp900838x
35. Jia W, Guo M, Zheng Z, Yu T, Rodriguez EG, Wang Y, Lei Y (2009) Electrocatalytic oxidation and reduction of H_2O_2 on vertically aligned Co_3O_4 nanowalls electrode: toward H_2O_2 detection. J Electroanal Chem 625(1):27–32. doi:10.1016/j.jelechem.2008.09.020
36. Qiu J, Peng HZ, Liang RP, Li J, Xia XH (2006) Synthesis, characterization, and immobilization of Prussian blue-modified Au nanoparticles: application to electrocatalytic reduction of H_2O_2. Langmuir 23(4):2133–2137. doi:10.1021/la062788q
37. Zeis R, Lei T, Sieradzki K, Snyder J, Erlebacher J (2008) Catalytic reduction of oxygen and hydrogen peroxide by nanoporous gold. J Catal 253(1):132–138. doi:10.1016/j.jcat.2007.10.017
38. Jalan V, Taylor EJ (1983) Importance of interatomic spacing in catalytic reduction of oxygen in phosphoric acid. J Electrochem Soc 130(11):2299–2302. doi:10.1149/1.2119574
39. de Lara González GL, Kahlert H, Scholz F (2007) Catalytic reduction of hydrogen peroxide at metal hexacyanoferrate composite electrodes and applications in enzymatic analysis. Electrochim Acta 52(5):1968–1974. doi:10.1016/j.electacta.2006.08.006